

Magnetism-driven unconventional effects in Ising superconductors: role of proximity, tunneling, and nematicity

Darshana Wickramaratne

*Center for Computational Materials Science, U.S. Naval Research Laboratory, Washington, DC 20375, USA**

Menashe Haim and Maxim Khodas

The Racah Institute of Physics, The Hebrew University of Jerusalem, Jerusalem 9190401, Israel

I.I. Mazin

*Department of Physics and Astronomy, George Mason University, Fairfax, VA 22030, USA and
Quantum Science and Engineering Center, George Mason University, Fairfax, VA 22030, USA*

(Dated: July 23, 2021)

Hybrid Ising superconductor-ferromagnetic insulator heterostructures provide a unique opportunity to explore the interplay between proximity-induced magnetism, spin-orbit coupling and superconductivity. Here we use a combination of first-principles calculations of NbSe₂/CrBr₃ heterostructures and an analytical theory of Ising superconductivity to analyze the existing experiments and provide a complete explanation of highly nontrivial and largely counterintuitive effects: an *increase* in the magnitude of the superconducting gap accompanied by the *broadening* of the tunneling peaks; hysteretic behavior of the tunneling conductance that sets in ≈ 2 K below T_c ; and nematic symmetry breaking in the superconducting state. The microscopic reason in all three cases appears to be the interplay between the proximity-induced exchange splitting and intrinsic defects. Finally, we predict additional interesting effects that at the moment cannot be addressed experimentally: spin-filtering when tunneling across CrBr₃ and tunneling “hot spots” in momentum space that are anticorrelated with regions where the spin-orbit splitting is maximum.

One of the most intriguing discoveries in superconductivity in the last decade is the so-called Ising superconductivity, which appears in materials without inversion symmetry and with a particular type of spin-orbit coupling (SOC) [1–6]. Thus far all experimental work on Ising superconductivity have been performed on single layers of the transition metal dichalcogenides (TMD), such as NbSe₂. Unlike conventional superconductors which can be classified by parity (centrosymmetric materials) or by the leading parity (non-centrosymmetric materials), Ising superconductivity represents a qualitatively different class, where each Cooper pair is described by an equal mix of singlet and triplet wave functions [4, 5]. This manifests in a range of unique properties which includes a theoretically infinite thermodynamical critical field along certain directions and nontrivial interplay of superconductivity with magnetism.

Combined with developments in the field of two-dimensional magnetic semiconductors [7, 8] this has motivated a large effort focused on using Ising superconductors in 2D Josephson junctions [9], or investigating tunneling across magnetic tunnel barriers [10–12]. Superconductor/ferromagnetic insulator junctions have, in particular, been used to elucidate the fundamental properties of the superconducting contacts and are also pursued for applications in spintronics [13] or hosting topological states [14–16].

Recent experiments [17–22] indicate that the behavior of Ising superconductor-magnetic insulator junctions is qualitatively different compared to conventional super-

conductors. Some of the most puzzling observations include hysteretic behavior in NbSe₂/Cr₂Ge₂Te₆ [20, 22] and in NbSe₂/CrBr₃/NbSe₂ heterostructures [21], which only appeared at ~ 2 K below T_c . Kang *et al* [21] convincingly demonstrated that the hysteresis, inexplicably, emerges from the Ising superconductor, and not from the ferromagnetic insulator. Refs. [17, 18] reported evidence of a two-fold rotation symmetry of the superconducting state, violating the three-fold symmetry of the hexagonal lattice of NbSe₂. Finally, Ref. [21] also found that as an external in-plane magnetic field rotates the CrBr₃ spins from being along \hat{z} to being in-plane, the superconducting gap, Δ , increases by $\sim 2\%$, while the broadening of the tunneling peak at the same time *also increases* by $\sim 50\%$. This is counterintuitive: one expects that when Δ increases the width of the tunneling peaks should decrease.

These experimental observations contain a lot of interpretative power and form a three-pronged puzzle that we will provide microscopic insight into in this study using a combination of first-principles calculations and analytical calculations based on a theory of Ising superconductivity that also accounts for spin-conserving scattering due to paramagnetic point defects [23–27].

We begin by examining the electronic structure of the NbSe₂/CrBr₃/NbSe₂ trilayer heterostructure using first-principles calculations [28]. The atomic structure of the heterostructure with the lowest energy is illustrated in Fig. 1(a). The alignment of the NbSe₂ states at the Fermi level at K with respect to the CrBr₃ spin up and spin

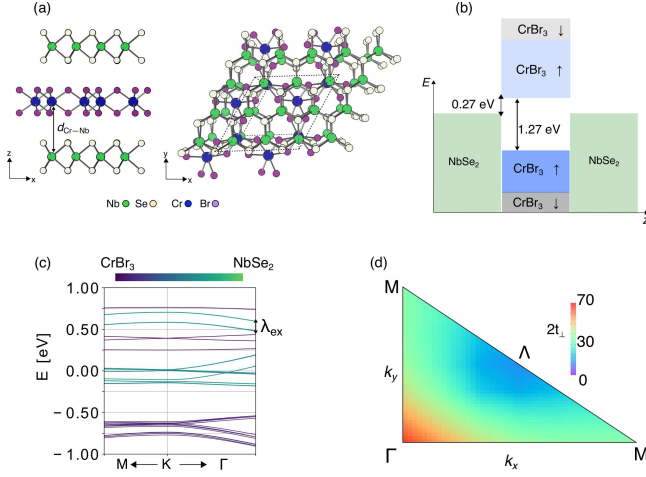


FIG. 1. (a) Trilayer heterostructure showing the side view and the top view. (b) Alignment of the energy levels of NbSe₂ with respect to monolayer CrBr₃ at the K-point. (c) Spin-polarized band structure of the trilayer heterostructure around the K point. (d) Interlayer coupling, $2t_{\perp}$, of the NbSe₂/CrBr₃/NbSe₂ trilayer heterostructure as a function of momentum. Λ corresponds to the Γ -K midpoint.

down states are illustrated in Fig. 1(b) and the spin-polarized band structure of the trilayer heterostructure is shown in Fig. 1(c). The NbSe₂ states reside within the spin-up gap of CrBr₃, close to the spin up conduction band states of CrBr₃.

One striking change in the electronic structure of the heterostructure is the large exchange splitting, λ_{ex} , of the NbSe₂ derived states (the bias field $\mu_B B = \lambda_{\text{ex}}/2$). For the heterostructure in Fig. 1(a), λ_{ex} is 121 meV between the spin up and spin down states. In bilayer NbSe₂, the two pairs of spin degenerate bands, contributed by each monolayer, are split due to interlayer coupling, t_{\perp} [28]. In the heterostructure calculations, the Nb atoms in the top and bottom monolayers acquire a magnetic moment, m_{Nb} , of ~ 0.10 to $0.13 \mu_B$ due to proximity induced Cr-Nb coupling. This manifests in a proximity induced exchange splitting, λ_{ex} , illustrated in Fig. 1(c), that breaks the spin degeneracy of these bands.

The magnitude of λ_{ex} reflects the magnitude of orbital overlap between the Nb and Cr d -electrons. It crucially depends on vertical separation distance between the Nb and Cr atoms, $d_{\text{Cr-Nb}}$ [28]. Moreover, as Fig. 1(b) illustrates, the quasiclassical tunneling barrier in the spin-majority channel is 0.27 eV, while it is several times larger in the spin-minority channel. Thus, we predict a strong spin-filtering effect for the Cr spins aligned along z with the spin-minority tunneling being strongly suppressed.

To form a commensurate trilayer heterostructure, we assume CrBr₃ layer is under biaxial tensile strain. In reality since the lattice mismatch is large, the two layers are incommensurate, which would lead to spatially

varying stacking of NbSe₂ with respect to CrBr₃. Given the strong itinerancy of Nb electrons, the lateral rigidity of both layers, the effective overlap and λ_{ex} should be averaged over all possible mutual orientations between the two layers, while the equilibrium distance corresponds to the sterically least favorable geometry, *i.e.*, when Br and Se ions are aligned vertically. The effect of this averaging [28] is that λ_{ex} at $d_{\text{Cr-Nb}} \approx 6.88 \text{ \AA}$ which, according to our calculations is the maximal possible separation distance between NbSe₂ and CrBr₃, becomes $\langle \lambda_{\text{ex}} \rangle \approx 0.04 \text{ meV}$, which is equivalent to a magnetic exchange field, $B \approx 0.7 \text{ T}$.

Inserting a single layer of CrBr₃ increases the interlayer separation between the NbSe₂ layers, which changes t_{\perp} . We illustrate the magnitude of $2t_{\perp}$ along Γ -M and along Γ - Λ (where Λ is the midpoint along the Γ -K path) in Fig. 1(d). Similar to the case of the NbSe₂ monolayers separated by vacuum [28], $t_{\perp}^{\Gamma} \gg t_{\perp}^{\text{K}}$. With two monolayers or more of CrBr₃ (as used by Kang *et al.* [21]), t_{\perp} at K is suppressed significantly compared to t_{\perp} at Γ [28].

Away from Γ , our calculations (Fig. 1(d) show that $2t_{\perp}$ along the diagonal (Γ -K), is lower compared to $2t_{\perp}$ along the Γ -M path. Note that the magnitude of the spin-orbit coupling (SOC) grows from Γ to Λ , while it is zero along Γ -M [4]. Hence, the orbitals that contribute the least to $2t_{\perp}$ leads to the largest Δ_{SOC} : the tunneling probability is correlated with the degree of the z^2 character of the Nb bands, while the SOC splitting is *anticorrelated* with it. This anticorrelation of the tunneling and SOC “hot spots” has crucial implications on interpreting tunneling measurements in these heterostructures, which we discuss next. Together with the spin filtering discussed above this constitutes another theoretical prediction that is yet to be verified by experiment.

Armed with this quantitative understanding of λ_{ex} , t_{\perp}^{Γ} , and t_{\perp}^{K} we proceed to perform model Hamiltonian calculations to describe tunneling across an Ising superconductor - ferromagnetic insulator - Ising superconductor junction [28]. We first consider, at a heuristic level, the impact of a magnetic exchange field that is out-of-plane (parallel to \hat{z}) and in-plane (parallel to \hat{x}) on the conductance peak. For a magnetic exchange field, B , that is out-of-plane ($B \parallel c$) the SOC and B both polarize the electron spins along \hat{z} regardless of the in-plane momentum. Hence, the magnetic exchange interaction reduces the energy of the singlet Cooper pairs, while SOC plays no role. This leads to a familiar Pauli limited superconductivity where the critical magnetic field is of the order of the gap, Δ [29]. Furthermore, the Cooper pairs retain their singlet identity and are immune to the disorder scattering in accordance with the Anderson theorem [30].

In contrast, when $B \perp c$, the impact on the order parameter is weak due to the strong Δ_{SOC} . However, the broadening of the conductance peak is sensitive to $B \perp c$ and grows with the magnitude of B . When

$B \perp c$, the spins acquire a finite in-plane momentum dependent component. The spin tilt angle is determined by Δ_{SOC} and therefore varies, with the in-plane momentum. Hence, the paramagnetic defects behave as magnetic defects due to a finite in-plane B [25, 27]. These qualitative considerations are summarized in Table I.

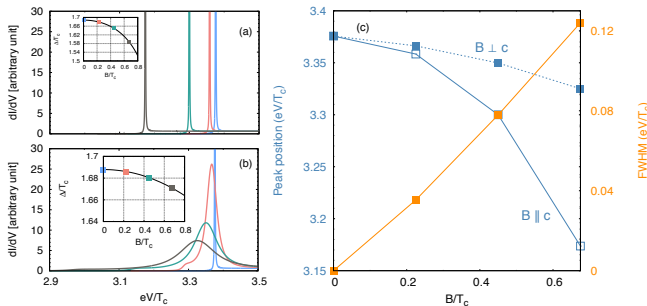


FIG. 2. Differential conductance dI/dV as a function of the bias voltage, $|e|V$ for an (a) out-of-plane magnetic field that is along \hat{z} ($B \parallel c$) and an (b) in-plane magnetic field that is along \hat{x} ($B \perp c$). We use four values of the magnetic exchange field, B that corresponds to $B = 0 T_c$ (blue), $0.225 T_c$ (red), $0.45 T_c$ (green), and $0.67 T_c$ (grey) to determine the change in differential conductance as a function of B . We use $T = 0.5T_c$, $\Delta_{\text{SOC}} = 20T_c$ and a scattering rate, $\eta = T_c$ for all of our differential conductance calculations. The inset in each panel (a) and (b) shows the suppression of the order parameter Δ_o as a function of B . (c) Change in the peak position of the differential conductance when $B \parallel c$ and $B \perp c$ (left vertical axis) and the change in the FWHM of the differential conductance as a function of $B \perp c$ (right vertical axis).

TABLE I. Parameters that control the position and broadening of the conductance peak as a function of the magnetic exchange field that is out-of-plane, $B \parallel c$ (for moderately low temperatures) and in-plane, $B \perp c$. B denotes the magnitude of the exchange field, Δ_o is the order parameter, Δ_{SOC} is the magnitude of spin-orbit coupling, and $\eta \ll \Delta_{\text{SOC}}$ is the disorder scattering rate.

| | $B \parallel c$ | $B \perp c$ |
|-----------------|------------------|--|
| peak shift | $(B/\Delta_o)^2$ | $(B/\Delta_{\text{SOC}})^2$ |
| peak broadening | 0 | $\eta B^2/(B^2 + \Delta_{\text{SOC}}^2)$ |

To put this on a firm theoretical footing we use a model band dispersion to describe the Γ -valley of monolayer NbSe₂ (since this is the valley through which most of the tunneling occurs!). We use this to calculate the order parameter for $B \parallel c$ and $B \perp c$ and combine this with the information from our first-principles calculations to determine the spin-dependent tunneling conductance [28].

The calculated dI/dV for an out-of-plane B is shown in Fig. 2(a). For each value of $B \parallel c$, we only find one dI/dV peak at $|e|V = 2\Delta_o$ which is not split by Zeeman coupling. This is due to the fact that the top and bottom NbSe₂ layers undergo the same amount of exchange

splitting, λ_{ex} [28]. Hence, the superconducting density of states is split by the same amount and spin is conserved during tunneling which leads to the single peak [31].

From Figure 2(a) it is evident that as the magnitude of B increases, the position of the dI/dV peak decreases. This is due to the suppression of the order parameter, Δ_o , which is proportional to B^2 . This is in contrast to the Zeeman split peaks in the density of states which shifts linearly with the magnitude of the exchange field. We also find that the full-width half maximum (FWHM) of the conductance peaks remains unchanged and is insensitive to the amount of disorder that we consider.

In Fig. 2(b) we illustrate the calculated dI/dV when $B \perp c$. We find a number of striking changes compared to Figure 2(a). The peak position of the dI/dV decreases and is weakly dependent on the magnitude of B . Secondly, the FWHM of the dI/dV increases as the magnitude of the in-plane B increases. This is consistent with the spin-flip scattering rate increasing quadratically as $\eta B^2/2\Delta_{\text{SOC}}^2$, where η is the scattering rate due to paramagnetic defects [25, 27].

In Figure 2(c) we summarize our calculations of the peak position and FWHM as a function of the magnitude and direction of B . These results confirm the qualitative analysis in Table I and provide a physically intuitive explanation for the modest increase in Δ , accompanied by the coherence peak broadening observed in tunneling measurements [21].

We now include two additional effects that are likely present in NbSe₂: magnetic point defects and extended defects. One candidate for magnetic point defects are Se vacancies, V_{Se} , which have been found in appreciable concentrations in NbSe₂ [23]. To verify this hypothesis we performed spin-unrestricted first-principles calculations of V_{Se} in a $(10 \times 10 \times 1)$ supercell. We find a sizeable magnetization ($\approx 0.6 \mu_B$, within our 300 atom supercell) and the induced magnetization has a finite length scale that is commensurate with the in-plane lattice constant ($\sim 15 \text{ \AA}$) of our large supercell as illustrated in Fig. 3(a). This is likely due to monolayer NbSe₂ being close to a magnetic instability [4, 32]. Interestingly, the induced spin-polarization is large and sign-changing, reminiscent of Friedel oscillations.

While we did not compute the magnetic anisotropy of such defects, it is likely to be easy-axis. Indeed, for an ideal hexagonal lattice, the symmetry allows for mixing of the $x^2 - y^2$ and xy Nb d -orbitals. This mixing can generate an orbital moment L_z , with no cost in kinetic energy. Hence, an isolated V_{Se} defect is likely to have its magnetic moment oriented along \hat{z} .

If the magnetic moment of the defect remains along \hat{z} , it has a pair breaking effect in the same way as it would in an ordinary s -wave superconductor. However, if it is aligned in-plane, this pair-breaking effect, within the Born approximation, becomes strongly anisotropic, leading to a considerable enhancement of the in-plane critical

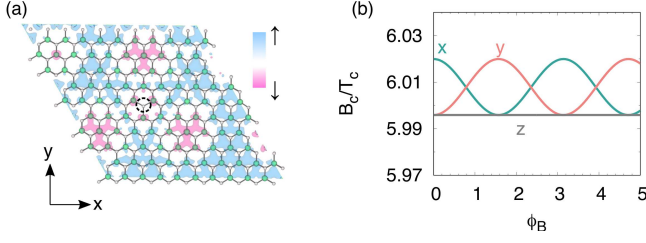


FIG. 3. (a) Spin density of a single selenium vacancy within a $10 \times 10 \times 1$ supercell of monolayer NbSe₂. The different colors correspond to different signs of the magnetization. The net magnetization is $\sim 0.6 \mu_B$. The position of the missing selenium atom is denoted with the black dotted circle. (b) The in-plane critical field, B_c as a function of the field orientation, specified by the angle ϕ_B formed by the magnetic field with respect to x -direction. We consider the magnetic easy axis of the defect spin along \hat{x} (green), \hat{y} (red) and \hat{z} (grey) with spin-flip scattering rates η_1, η_2 and η_3 equal to $0.25 T_c$. We set $T = 0.2 T_c$ and $\Delta_{\text{SOC}} = 20 T_c$.

field in the in-plane direction parallel to the impurity moment. [26]. In Fig. 3(b) we illustrate the in-plane critical field as a function of the orientation of $B \perp c$. Note the two-fold oscillations for an in-plane defect spin.

The finite spatial extent of the magnetization, R_d , due to V_{Se} , also provides a plausible explanation for the puzzling hysteresis in the tunneling conductance that occurs at $T \lesssim (T_c - 2\text{K})$ [21]. As the temperature is lowered below T_c , the superconducting coherence length, ξ , decreases and at some point may become lower than R_d . When $\xi < R_d$, scattering would occur within the unitary limit which would result in superconductivity being suppressed near the vacancy, within a length of the order of R_d . This suppression only occurs when the magnetic moment of the defect is oriented along \hat{z} (as discussed above, this is likely the case for isolated V_{Se}). When the pairing energy of the resulting “puddle” of finite magnetization, which is $\sim \Delta^2 N(0) R_d^2$, becomes larger than the magnetic anisotropy energy (typically on the order of μeV for point defects), the magnetic moment of the point defect would flop to be in-plane. We expect this behavior to be hysteretic, as is typical for a magnetic transition.

So far we have considered point defects. However, as-grown NbSe₂ is known to exhibit extended defects such as grain boundaries [24] and dislocations. Elastic fields tend to align linear defects along the same direction, which would break the global C_3 symmetry of the hexagonal lattice. The strain fields that manifest from extended defects have been proposed to affect the symmetry of the superconducting state [33]. Below we present an alternative mechanism on how extended defects might break the C_3 symmetry in the superconducting state.

At first glance it seems that this would require a “nematic” superconducting order parameter, that intrinsically breaks the C_3 symmetry [17, 18]. While this would, by definition, generate the desired symmetry breaking,

it also implies that the expected s -wave state is nearly degenerate with some other state(s) with a different pairing symmetry. This is a logical assumption in materials like the Fe-based superconductors, where the same spin-fluctuations generate pairing in the s_{\pm} and a d channel, so it is not surprising that a combination of both may be energetically favorable. In the superconducting TMDs, on the other hand, spin or Coulomb interactions are pair-breaking in the s -wave channel. As a result, the competition between conventional and unconventional pairing mechanisms requires an extremely fine tuning of parameters, and a dramatic difference between the bulk and the single layer pairing mechanism. In addition, one must assume that the interactions are extremely sensitive to the small strain generated by the extended defects or externally.

In this context, an interesting question to ask is: can symmetry-breaking extended defects result in a tunneling conductance and critical field that has C_2 symmetry with respect to the direction of the external magnetic field *without impacting the symmetry of the superconducting order parameter*? To this effect, we observe that while an isolated point defect (vacancy) is expected to have its spin aligned with the z -axis, the same does not hold near an extended defect, where the local C_3 symmetry is broken and the d -orbitals of the Nb dangling bond states can mix. In this case the orbital magnetic moment can point along an in-plane direction determined by the linear defect.

According to our theory, the defect-induced broadening of the tunneling peaks and the pair breaking by the magnetic field will depend on the angle between the direction of the applied magnetic field and the orientation of the extended defect within the basal plane of NbSe₂. The extended defects broaden the superconducting density of states near the conductance peak, break the C_3 rotational symmetry at or slightly below T_c , in agreement with the existing experimental observations [17, 18]. If these point defects have a finite magnetic moment, they can also indirectly trigger an anisotropy in the magnetoresistance near T_c by generating an easy-axis magnetic anisotropy of the defect.

This provides an immediate explanation of the π -periodic angular dependence (*i.e.*, a C_2 rather than C_3 symmetry) the in-plane magnetoresistance either in the transition region centered at T_c [17] or slightly below T_c [18], without invoking an *ad hoc* assumption about nematic superconductivity (admittedly, our interpretation assumes an in-plane easy axis for magnetic defects pinned to extended defects, but this is plausible from a materials science point of view.)

In summary, using first-principles calculations and an analytical theory for Ising superconductivity we have systematically investigated proximity induced effects in NbSe₂/CrBr₃ heterostructures. We find CrBr₃ leads to a proximity-induced exchange splitting of the NbSe₂ states

and that the NbSe₂ states at Γ contribute the most to tunneling. Scattering of the NbSe₂ states at Γ off of paramagnetic point defects leads to a pronounced broadening of the tunneling peaks, a modest enhancement of the superconducting gap when the magnetic exchange field is in-plane. Within the same framework, extended linear defects generate two-fold oscillations of the critical field, seen in experiments. Finally, we find point defects such as selenium vacancies acquire a finite magnetization of a sizeable length scale, which can explain the finite hysteresis in the conductance. Last but not least, we predict two effects that can be verified by future experiments (and may have more theoretical ramifications than discussed here): spin-filtering when tunneling through the CrBr₃ barrier and anticorrelation between the SOC and the tunneling probability.

We thank David Möckli, Jie Shan, Kin Fai Mak and Rafael Fernandes for helpful discussions. D.W. was supported by the Office of Naval Research through the Naval Research Laboratory's Basic Research Program. I.I.M. was supported by ONR through grant N00014-20-1-2345. M.H. and M.K. acknowledge the financial support from the Israel Science Foundation, Grant No. 2665/20. Calculations by D.W. and I.I.M. were performed at the DoD Major Shared Resource Center at AFRL.

* darshana.wickramaratne@nrl.navy.mil

- [1] J. Lu, O. Zheliuk, I. Leermakers, N. F. Yuan, U. Zeitler, K. T. Law, and J. Ye, *Science* **350**, 1353 (2015).
- [2] X. Xi, Z. Wang, W. Zhao, J.-H. Park, K. T. Law, H. Berger, L. Forró, J. Shan, and K. F. Mak, *Nat. Phys.* **12**, 139 (2016).
- [3] C. Sergio, M. R. Sinko, D. P. Gopalan, N. Sivadas, K. L. Seyler, K. Watanabe, T. Taniguchi, A. W. Tsen, X. Xu, D. Xiao, and B. Hunt, *Nat. Comm.* **9**, 1427 (2018).
- [4] D. Wickramaratne, S. Khmelevskiy, D. F. Agterberg, and I. I. Mazin, *Phys. Rev. X* **10**, 041003 (2020).
- [5] D. Shaffer, J. Kang, F. Burnell, and R. M. Fernandes, *Phys. Rev. B* **101**, 224503 (2020).
- [6] G. Tang, C. Bruder, and W. Belzig, *Phys. Rev. Lett.* **126**, 237001 (2021).
- [7] M. A. McGuire, *Crystals* **7**, 121 (2017).
- [8] H. H. Kim, B. Yang, S. Li, S. Jiang, C. Jin, Z. Tao, G. Nichols, F. Sfigakis, S. Zhong, C. Li, S. Tian, D. Cory, G.-X. Miao, J. Shan, K. F. Mak, H. Lei, K. Sun, L. Zhao, and A. Tsen, *Proc. Natl. Acad. Sci. U.S.A* **116**, 11131 (2019).
- [9] T. Dvir, F. Massee, L. Attias, M. Khodas, M. Aprili, C. H. Quay, and H. Steinberg, *Nature communications* **9**, 1 (2018).
- [10] T. Tokuyasu, J. A. Sauls, and D. Rainer, *Phys. Rev. B* **38**, 8823 (1988).
- [11] P. Tedrow, J. Tkaczyk, and A. Kumar, *Phys. Rev. Lett.* **56**, 1746 (1986).
- [12] T. T. Heikkilä, M. Silaev, P. Virtanen, and F. S. Bergeret, *Progress in Surface Science* **94**, 100540 (2019).
- [13] M. Eschrig, *Reports on Progress in Physics* **78**, 104501 (2015).
- [14] J. D. Sau, S. Tewari, and S. D. Sarma, *Phys. Rev. B* **85**, 064512 (2012).
- [15] S. Głodzik and T. Ojanen, *New Journal of Physics* **22**, 013022 (2020).
- [16] S. Kezilebieke, M. N. Huda, V. Vaño, M. Aapro, S. C. Ganguli, O. J. Silveira, S. Głodzik, A. S. Foster, T. Ojanen, and P. Liljeroth, *Nature* **588**, 424 (2020).
- [17] A. Hamill, B. Heischmidt, E. Sohn, D. Shaffer, K.-T. Tsai, X. Zhang, X. Xi, A. Suslov, H. Berger, L. Forró, *et al.*, *Nature Physics*, 1 (2021).
- [18] C. woo Cho, J. Lyu, T. Han, C. Y. Ng, Y. Gao, G. Li, M. Huang, N. Wang, J. Schmalian, and R. Lortz, *arXiv preprint arXiv:2003.12467* (2020).
- [19] H. H. Kim, B. Yang, S. Tian, C. Li, G.-X. Miao, H. Lei, and A. W. Tsen, *Nano Lett.* **19**, 5739 (2019).
- [20] H. Idzuchi, F. Pientka, K.-F. Huang, K. Harada, Ö. Gül, Y. Shin, L. Nguyen, N. Jo, D. Shindo, R. Cava, *et al.*, *arXiv preprint arXiv:2012.14969* (2020).
- [21] K. Kang, S. Jiang, H. Berger, K. Watanabe, T. Taniguchi, L. Forró, J. Shan, and K. F. Mak, "Giant anisotropic magnetoresistance in Ising superconductor-magnetic insulator tunnel junctions," (2021), [arXiv:2101.01327 \[cond-mat.supr-con\]](https://arxiv.org/abs/2101.01327).
- [22] L. Ai, E. Zhang, C. Huang, X. Xie, Y. Yang, Z. Jia, Y. Zhang, S. Liu, Z. Li, P. Leng, *et al.*, *arXiv preprint arXiv:2101.04323*.
- [23] L. Nguyen, H.-P. Komsa, E. Khestanova, R. J. Kashtiban, J. J. Peters, S. Lawlor, A. M. Sanchez, J. Sloan, R. V. Gorbachev, I. V. Grigorieva, *et al.*, *ACS Nano* **11**, 2894 (2017).
- [24] H. Wang, X. Huang, J. Lin, J. Cui, Y. Chen, C. Zhu, F. Liu, Q. Zeng, J. Zhou, P. Yu, *et al.*, *Nat. Comm.* **8**, 1 (2017).
- [25] E. Sosenko, J. Zhang, and V. Aji, *Phys. Rev. B* **95**, 144508 (2017).
- [26] D. Möckli, M. Haim, and M. Khodas, *Journal of Applied Physics* **128**, 053903 (2020).
- [27] M. Haim, D. Möckli, and M. Khodas, *Physical Review B* **102**, 214513 (2020).
- [28] See Supplemental Material at [url] for additional electronic structure calculations of the trilayer heterostructure, the derivation of the free energy of the order parameter for a magnetic exchange field that is applied parallel to the plane of the heterostructure, and includes Refs. [34-43].
- [29] K. Maki and T. Tsuneto, *Progress of Theoretical Physics* **31**, 945 (1964).
- [30] P. W. Anderson, *Journal of Physics and Chemistry of Solids* **11**, 26 (1959).
- [31] R. Meservey and P. Tedrow, *Physics reports* **238**, 173 (1994).
- [32] S. Divilov, W. Wan, P. Dreher, E. Bölen, D. S. Portal, M. M. M. Ugeda, and F. Yndurain, *Journal of Physics: Condensed Matter* (2021).
- [33] R. Willa, M. Hecker, R. M. Fernandes, and J. Schmalian, (2020), [arXiv:2011.01941 \[cond-mat.supr-con\]](https://arxiv.org/abs/2011.01941).
- [34] P. E. Blöchl, *Phys. Rev. B* **50**, 17953 (1994).
- [35] G. Kresse and J. Hafner, *Phys. Rev. B* **47**, 558 (1993).
- [36] G. Kresse and J. Furthmüller, *Phys. Rev. B* **54**, 11169 (1996).
- [37] J. P. Perdew, K. Burke, and M. Ernzerhof, *Phys. Rev. Lett.* **77**, 3865 (1996).

- [38] S. Grimme, J. Antony, S. Ehrlich, and H. Krieg, J. Chem. Phys. **132**, 154104 (2010).
- [39] S. Grimme, J. Comput. Chem. **27**, 1787 (2006).
- [40] S. Grimme, S. Ehrlich, and L. Goerigk, J. Comput. Chem. **32**, 1456 (2011).
- [41] J. Klimeš, D. R. Bowler, and A. Michaelides, Phys. Rev. B **83**, 195131 (2011).
- [42] L. Handy and N. Gregory, Journal of the American Chemical Society **74**, 891 (1952).
- [43] I. Mazin, EPL (Europhysics Letters) **55**, 404 (2001).